Three-Dimensional Transmission Electron Microscopic Observations of Mesopores in Dealuminated Zeolite Y**

Andries H. Janssen, Abraham J. Koster, and Krijn P. de Jong*

Zeolites are microporous crystalline aluminosilicates, which makes them very suitable for separation processes or shape-selective catalysis. The micropores of zeolites often induce advantageous shape selectivity, but enhanced accessibility is frequently desirable to restrict mass-transfer effects and/or allow catalytic conversion of larger molecules. Several approaches have been followed to enhance accessibility,[1] such as the development of zeolites with intrinsically larger pores,[2] delaminated zeolite precursors,[3] and zeolite nanocrystals.[4] A widely applied method to enhance accessibility is the creation of materials with both micropores (< 2 nm diameter) and mesopores ($2 – 50$ nm diameter). This can be done by special synthetic techniques[5] or by postsynthetic modification of zeolites with hydrothermal treatment (steaming) or acid leaching.[6] Steaming and acid-leaching treatments generate mesopores by extracting aluminum from the zeolite lattice, thus causing a partial collapse of the framework. Up to now, the characterization of these mesopores has been done with nitrogen physisorption and transmission electron microscopy (TEM).[7] However, the visualization of the mesopores with conventional TEM gives no information about the shape, connectivity, and three-dimensional orientation of the pores. Furthermore, the zeolite crystals are often cut into thin slices with an ultramicrotome to investigate the pores. This may fracture the zeolite crystal, which hinders the interpretation of the TEM images. Recently, the mesoporous structure of MCM-48 has been determined by electron crystallography.[8] However, this method is suitable only for materials with well ordered pores. With three-dimensional transmission electron microscopy (3D-TEM) it is possible to image (random) mesopores of an intact zeolite crystal in three dimensions.[9] Herein, we show 3D-TEM results of the size, shape, and connectivity of the mesopores in a series of (steamed/acid-leached) Y zeolites. Moreover, a quantitative comparison between the 3D-TEM images and nitrogen physisorption is made. This enables us to propose a detailed model for the generation of mesopores.

[*] Prof. Dr. Ir. K. P. de Jong, Dr. A. H. Janssen
Department of Inorganic Chemistry and Catalysis
Debye Institute, Utrecht University
PO Box 80083, 3508 TB Utrecht (The Netherlands)
Fax: (+31) 30-251-1027
E-mail: k.p.dejong@chem.uu.nl

Dr. A. J. Koster
Department of Molecular Cell Biology
Utrecht University
Padualaan 8, 3584 CH Utrecht (The Netherlands)

3D-TEM, sometimes referred to as electron tomography,[10] is a technique in which a series of 2D TEM images (scattering contrast) is recorded, that is subsequently used to compute a 3D image (3D reconstruction) of the investigated object.[9–12] By virtual cross-sectioning of such a 3D reconstruction, one can reveal the interior of the object. To study the generation of mesopores, we used a series of Y zeolites with increasing mesopore volume, namely, NaY, USY (Ultra Stable Y), and XVUSY (eXtra Very Ultra Stable Y). The USY sample is a steamed NH_4Y, whereas the XVUSY is steamed twice and extensively acid leached. The physical properties of these samples are given in Table 1.

Table 1. Physical properties of NaY (CBV100), USY (CBV400) and XVUSY (CBV780)

	Si/Al bulk [at/at]	Si/Al XPS [at/at]	a_0 [nm]	% Y[a]	V_{micro}[b] [mL g^{-1}]	V_{micro}^{calcd}[c] [mL g^{-1}]	V_{meso}[d] [mL g^{-1}]	S_T[e] [m^{2}g^{-1}]
NaY	2.6	2.8	2.469	100	0.341	0.341	0.053	8
USY	2.6	1.1	2.450	87	0.256	0.324	0.108	63
XVUSY	39.3	71.3	2.423	72	0.277	0.267	0.251	120

[a] Relative crystallinity. [b] Micropore volume from t-plot: $t = [14.3600/(0.1013 - \lg(P/P_0))]^{0.5}$. [c] Expected micropore volume if all micropores are empty; calculated by correcting V_{micro} of NaY for crystallinity, a_0, and sodium mass of USY and XVUSY. [d] $V_{total} - V_{micro}$. [e] Sum of external and mesopore surface area calculated from t-plot.[13]

In Figures 1 – 3, 2D-TEM images and thin slices through the 3D-TEM reconstructions are shown for NaY, USY, and XVUSY, respectively (all scale bars represent 200 nm). In the
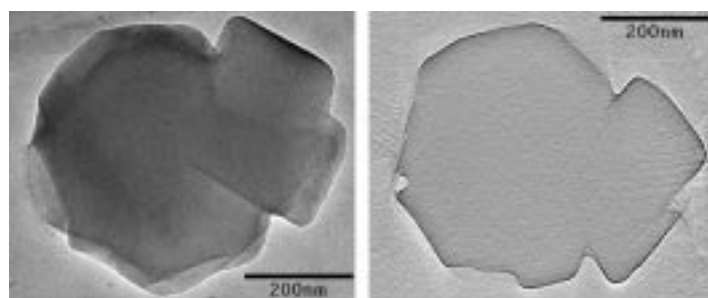

Figure 1. a) 2D-TEM image of a NaY crystal taken at a magnification of $\times 15$k and b) a thin (1.7 nm) slice through the 3D-TEM reconstruction of this crystal.

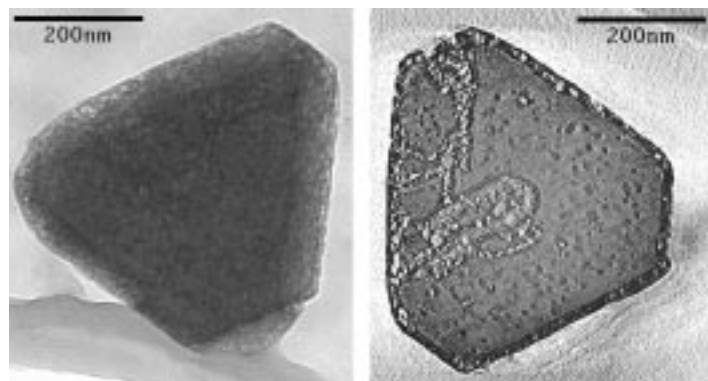

Figure 2. a) 2D-TEM image of a USY crystal taken at a magnification of $\times 15$k and b) a thin (1.7 nm) slice through the 3D-TEM reconstruction of this crystal.
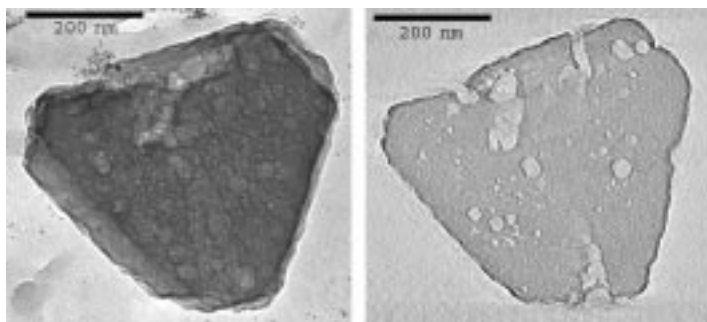
Figure 3. a) 2D-TEM image of an XVUSY crystal taken at a magnification of ×20k and b) a thin (1.25 nm) slice through the 3D-TEM reconstruction of this crystal. Small gold particles (5 nm), used as markers, are observed in Figure 3a.

conventional TEM images, the mesopores of USY and XVUSY are just visible as lighter areas, whereas, in the thin slices through the 3D-TEM reconstructions of USY and XVUSY, the mesopores can be distinguished very well as light areas. In line with the physisorption results (Table 1), NaY does not show any mesopores in both the 2D- and 3D-TEM images; the same holds for NH_4Y (not shown). This indicates that the light areas in Figure 2b and 3b really are the mesopores and not an artifact of the reconstruction. The diameters of the mesopores visualized with 3D-TEM are 3–20 nm for USY and 4–34 nm for XVUSY. This is in excellent agreement with the pore-size distributions calculated from the nitrogen desorption isotherms: 4–20 nm and 4–40 nm for USY and XVUSY, respectively. The large porous area in the USY crystal (Figure 2b, center left) is not a single pore but consists of many small cavities separated by thin walls. This explains why no pores larger than 20 nm are found from the nitrogen adsorption–desorption experiments. The 3D-TEM reconstructions also show that in USY and XVUSY the majority of the mesopores are cavities, although there are also some cylindrical pores connecting the outer surface with the interior of the zeolite crystallite. The shape of the hysteresis loop in the nitrogen physisorption isotherms of USY and XVUSY is indicative for inkbottle-type pores combined with cylindrical pores. The cavities visualized with 3D-TEM are most likely connected to the microporous system of the zeolite, thus giving inkbottle type adsorption–desorption behavior in physisorption.

In the cross-section of the 3D-TEM reconstruction of the USY crystal (Figure 2b), some dark cavities (5–20 nm diameter) and a dark band (about 15 nm thick) on the outer surface are also visible. TEM studies have shown that the dark areas inside and outside the crystals of steamed zeolites are most likely amorphous alumina deposited in the mesopores and on the external surface during the steaming process.[7a–c, 14] Therefore, we believe that the dark areas in our 3D-TEM reconstruction are not artifacts of the reconstruction but the imaging of confined material in the mesopores and amorphous alumina deposited on the external surface. In the XVUSY sample, no confined material could be detected (Figure 3b) because this has been removed during the severe acid-leaching step. When the bulk Si/Al ratio is compared with the surface Si/Al ratio obtained with XPS (Table 1), it is

clear that only for USY is there an enrichment of the external surface of the crystals with aluminum. This supports our 3D-TEM observations that only for USY there is a dark band of amorphous alumina on the external surface.

From the 3D-TEM observations, we propose a detailed model for the generation of mesopores in dealuminated zeolite Y (see Figure 4). The model largely supports earlier
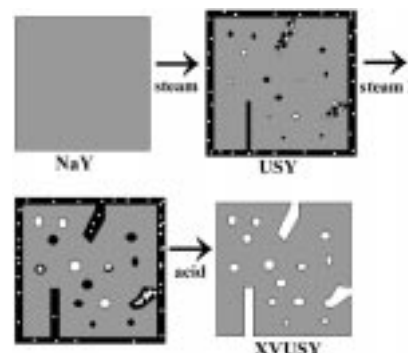

Figure 4. Model for the generation of mesopores in zeolite Y. The zeolite is gray, the amorphous alumina is black, and the empty mesopores are white.

ones[7a–c, 15] but adds key aspects of mesopore generation. During the steaming process (from NH_4Y to USY), aluminum ions are extracted from the zeolite lattice and deposited in the micro- and mesopores and on the external surface of the crystals.[16] This is confirmed by the decrease of the zeolite unit cell, the dark areas in the cross-sections of the 3D-TEM reconstruction of USY, and the surface enrichment with aluminum of the USY sample as observed with XPS (Table 1). The measured micropore volume for USY is lower than the value expected if all micropores were empty (Table 1; V_{micro} versus V_{micro}^{calcd}), which indicates that confined material is also present in the micropores. During the extraction of aluminum from the lattice, mobile silicon species from defect sites (where aluminum has been extracted) cause some defect sites to develop into cavities in the zeolite crystals and other defect sites to vanish by healing the framework. The volume and shape of the mesopores, determined by nitrogen physisorption and 3D-TEM, confirm this cavity-formation mechanism. Thus, the mesoporous system is primarily formed through cavities inside the crystals and not through pores connecting the interior of the crystals with the external surface. During the second steaming step in the generation of XVUSY, small cavities close to one another (as visible in Figure 2b) form larger cavities and cylindrical pores, which can be seen from the nitrogen physisorption measurements and 3D-TEM reconstructions. By acid leaching of the steamed sample, extra-framework aluminum species in the micro- and mesopores and on the external surface area dissolve.[6, 14] This is confirmed by the 3D-TEM reconstruction of XVUSY, which shows neither any confined material in the mesopores nor amorphous alumina on the external surface. Furthermore, XPS shows no surface enrichment in aluminum for XVUSY and the measured and "expected" micropore volume (Table 1) are comparable. Despite the development of a mesopore system, 2D- and 3D-TEM images show that the crystals

remain intact during the steaming and acid-leaching steps. Furthermore, the pore-size distribution from the nitrogen-desorption isotherm of all three samples shows an additional peak at a pore diameter of 70 nm. That this peak, which is caused by the interstitial space between the crystals, is at the same position for all three samples indicates that the crystals of these samples are of the same order of magnitude. This is different from the results obtained by Beyerlein et al.,[7a–c] who claimed extensive fracturing of zeolite Y crystals.

Thus, the pores in a series of dealuminated zeolite Y have been imaged in order to gain insight in the shape and three-dimensional ordering of the mesopores in the zeolite crystallites. Based on the surprising result, that most of the mesopores are present as cavities rather than cylindrical pores connecting the external surface with the interior of the crystallite, a more detailed model for the generation of these mesopores is proposed. However, the shape of the mesopores also raises the question to what extent the accessibility and diffusion are enhanced by the formation of these cavities.

Experimental Section

Samples CBV100 (NaY), CBV400 (USY), and CBV780 (XVUSY) were obtained from Shell International Chemicals and Zeolyst. Nitrogen adsorption and desorption measurements (Micromeritics ASAP 2010) were performed at liquid nitrogen temperature. XPS measurements (Vacuum Generators XPS) were performed on a system using nonmonochromatic $Al_{K\alpha}$ radiation at an anode current of 20 mA at 10 keV. For electron microscopy, a droplet of a colloidal gold suspension (Sigma, 5 nm gold) was dried on a carbon-coated copper grid, thus providing markers for the alignment of the data set. Next, a droplet of a suspension of the sample in ethanol was dried on this grid. From a representative crystal, a tilt series of about 141 images was taken from about $+70°$ to $-70°$ at 1° intervals of magnification $\times 15$ k or $\times 20$ k on one of two microscopes (Philips CM 200 FEG or a Tecnai 20) at 200 kV and with software for automated electron tomography.[12] From the tilt series, a 3D-reconstruction of the crystal is calculated as a stack of thin (1–2 nm) slices.[9–12]

Received: October 20, 2000 [Z15971]

[1] J. M. Thomas, *Angew. Chem.* **1999**, *111*, 3800–3843; *Angew. Chem. Int. Ed.* **1999**, *38*, 3588–3628.
[2] C. C. Freyhardt, M. Tsapatsis, R. F. Lobo, K. Balkus, Jr., M. E. Davis, *Nature* **1996**, *295*, 295–298.
[3] A. Corma, V. Fornes, S. B. Pergher, T. L. M. Maesen, J. G. Buglass, *Nature* **1998**, *396*, 353–356.
[4] S. Mintova, N. H. Olson, V. Valtchev, T. Bein, *Science* **1999**, *283*, 958–960.
[5] C. J. H. Jacobsen, C. Madsen, J. Houzvicka, I. Schmidt, A. Carlsson, *J. Am. Chem. Soc.* **2000**, *122*, 7116–7117.
[6] J. Scherzer, *ACS Symp. Ser.* **1984**, *248*, 157.
[7] a) C. Choi-Feng, J. B. Hall, B. J. Huggins, R. A. Beyerlein, *J. Catal.* **1993**, *140*, 395–405; b) C. Choi-Feng, J. B. Hall, B. J. Huggins, R. A. Beyerlein, *ACS Symp. Ser.* **1994**, *571*, 81–97; c) R. A. Beyerlein, C. Choi-Feng, J. B. Hall, B. J. Huggins, G. J. Ray, *Top. Catal.* **1997**, *4*, 27–42; d) Y. Sasaki, T. Suzuki, Y. Takamura, A. Saji, H. Saka, *J. Catal.* **1998**, *178*, 94–100.
[8] A. Carlsson, M. Kaneda, Y. Sakamoto, O. Terasaki, R. Ryoo, S. H. Joo, *J. Electron Microsc.* **1999**, *48*, 795–798.
[9] A. J. Koster, U. Ziese, A. J. Verkleij, A. H. Janssen, K. P. de Jong, *J. Phys. Chem. B* **2000**, *104*, 9368–9370.
[10] J. Frank, *Electron Tomography*, Plenum, New York, **1992**.
[11] A. J. Koster, U. Ziese, A. J. Verkleij, A. H. Janssen, J. de Graaf, J. W. Geus, K. P. de Jong, *Stud. Surf. Sci. Catal.* **2000**, *130*, 329–334.
[12] A. J. Koster, R. Grimm, D. Typke, R. Hegerl, A. Stoschek, J. Walz, W. Baumeister, *J. Struct. Biol.* **1997**, *120*, 276–308.
[13] P. Hudec, J. Novansky, S. Silhar, T. N. Trung, M. Zubek, J. Madar, *Adsorpt. Sci. Technol.* **1986**, *3*, 159–166.
[14] J. Lynch, F. Raatz, P. Dufresne, *Zeolites* **1987**, *7*, 333–340.
[15] C. Marcilly, *Pet. Tech.* **1986**, *328*, 12–18.
[16] M. J. Remy, D. Stanica, G. Poncelet, E. J. P. Feijen, P. J. Grobet, J. A. Martens, P. A. Jacobs, *J. Phys. Chem. B* **1996**, *100*, 12240–12447.

Fluorescence Detection of Specific RNA Sequences Using 2′-Pyrene-Modified Oligoribonucleotides**

Kazushige Yamana,* Hirofumi Zako, Kentarou Asazuma, Reiko Iwase, Hidehiko Nakano, and Akira Murakami

Fluorescence detection of specific RNA sequences is an area of much current interest and activity. It is important for the investigation of the regulatory mechanisms of gene expression[1, 2] and diagnostic analysis of infectious organisms from viruses or bacteria.[3, 4] Recent works have focused on the design and synthesis of fluorescent oligonucleotides that exhibit an enhanced signal upon hybrid formation,[5–14] since these type of probes can be used in homogeneous, as well as heterogeneous, assays. The enhanced fluorescence has facilitated monitoring in vitro transcription,[15] ribozyme reaction,[16, 17] and RNA folding.[18]

Our research efforts have concentrated on the use of the sugar 2′-position as the site in the covalent attachment of several fluorophores.[19–22] In particular, the incorporation of pyrene, via a one carbon-atom linker, into the specified position of oligodeoxyribonucleotides has provided a probe that exhibits strong fluorescence upon binding to RNA.[21, 22] While the potential of these probes is appreciated, it has remained unfulfilled because the pyrene–DNA complexes are plagued by the sequence limitation of the probe or the positioning of C or G bases at the 3′-site of the pyrene modification to gain a measurably strong fluorescence.[22] We now disclose a new pyrene probe derived from RNA that overcomes this limitation. The pyrene fluorescence is signifi-

[*] Assoc. Prof. K. Yamana, H. Zako, K. Asazuma, Prof. H. Nakano
Department of Applied Chemistry
Himeji Institute of Technology
2167 Shosha, Himeji, Hyogo 671-2201 (Japan)
Fax: (+81) 792-67-4895
E-mail: yamana@chem.eng.himeji-tech.ac.jp
Dr. R. Iwase, Prof. A. Murakami
Department of Polymer Science and Engineering
Kyoto Institute of Technology
Matsugasaki, Sakyo-ku, Kyoto 606-8585 (Japan)

Supporting information for this article is available on the WWW under http://www.angewandte.com or from the author.